Performance Optimization of 2-PolSK in UV Scattering Communication Channels

Srishti Sharma and and Swades De

***Abstract*—In this paper, we investigate the performance improvement of binary polarization shift keying (2-PolSK) transmission over the ultraviolet scattering channels. To this end, we statistically characterize the cross-polarization discrimination (XPD) of the channel when horizontal and vertical polarization are individually transmitted. The received polarization is characterized in terms of its statistical moments and approximating it to be truncated Gaussian distributed. To enhance 2-PolSK error performance, we propose XPD-dependent optimal thresholding. Electric field Monte Carlo (EFMC) simulation is used to realize the channel. The bit error rate results show a significant improvement through our proposed approach as compared to the conventional symmetric thresholding-based signal reception.**

***Index Terms*—UV scattering channels, cross-polarization discrimination, binary polarization shift keying, thresholding**

I. Introduction

Optical wireless communication has gained prominence for its abundant spectral resources, high data rates, immunity to electromagnetic interference, and use of low-power transceivers. Solar blind feature at the ground level and the ability to communicate via non-line of sight (NLOS) paths make deep ultraviolet (UV) (200 $\sim$ 300 nm) band preferable over visible light and infrared bands. UV NLOS propagation occurs due to strong molecular and aerosol scattering effects which act as a medium for information exchange.

Various modulation techniques were proposed for UV NLOS communication. On-off keying (OOK), pulse position modulation (PPM), and multi-PPM were studied in [1], [2]. Digital and dual-head pulse interval [3], 4-frequency shift keying [4], orbital angular momentum [5], binary phase shift keying subcarrier intensity [6], and M-ary spectral amplitude code [7] modulations were shown to outperform OOK and PPM. Yet, *polarization*-aware UV NLOS communication is of interest because unlike amplitude and angle modulations, it is insensitive to path loss and phase noise; only sufficient power level is required for symbol detection.

The propagation of polarized light in scattering environments (turbid media, tissues) was studied using electric field Monte Carlo (EFMC) [8], [9] simulations and MC-based Stokes-Muller transformations [10]. They did not study the communication performance over the scattering channels. To address this lacuna, the feasibility of NLOS polarized UV communication was studied in [11]. Dual (intensity and polarization) modulation [12] and polarization multiplexing [13] were proposed in UV communication. Thus, combining the existing modulation schemes with binary polarization shift keying (2-PolSK) can double the achievable data rate. However, polarization-aware communication performance in scattering channel has not been sufficiently studied in literature.

The authors are with the Department of Electrical Engineering, Indian Institute of Technology Delhi, New Delhi, India (e-mail: srishti.sharma@ee.iitd.ac.in, swadesd@ee.iitd.ac.in).

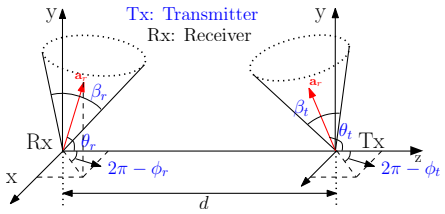

Fig. 1 Geometrical setup for photon propagation in scattering channel.

In this paper, we aim to improve the performance of 2-PolSK transmission over UV scattering channels by exploiting the asymmetric cross-polarization discrimination (XPD) of horizontal and vertical polarized signal components and devising an XPD-dependent symbol detection strategy. The following key contributions are made: (1) XPD-based scattering channel characterization and XPD-dependent polarization orientation are mathematically captured. (2) Different scattering channel scenarios are defined in terms of polarization orientation variance, and conditions are obtained under which different-from-conventional symmetric thresholding is required for minimum error performance. (3) Optimal thresholding is decided by modeling the received polarization orientation as truncated Gaussian distributed. Expectation maximization (EM) algorithm is used to compute the modeled statistical parameters. Optimal thresholds are derived in terms of the statistical moments of the received signal polarization. (4) EFMC based polarized light propagation and condition for its reception are discussed, and the BER performance of the proposed optimal thresholding is compared with respect to the conventional symmetric thresholding.

Remark 1. *In this work, 2-PolSK is achieved by transmitting either horizontal (vector along x axis) or vertical (vector along y axis) polarization from the transmitter.*

II. System Model

In the absence of LOS path between a transmitter-receiver pair, scattering can offer NLOS path for communication. Fig. 1 shows NLOS UV link geometry with a polarized transmitter and receiver positioned, respectively, at $\mathbf{s}_t = (0, 0, d)$ and $\mathbf{s}_r = (0, 0, 0)$ in the considered inertial frame of reference. β_t is the transmitter beam full-width divergence, β_r is the receiver field of view (FOV) angle, θ_t (θ_r) and ϕ_t (ϕ_r) are respectively the elevation and azimuth angles for the transmitted light beam (receiver). d is the transmitter-receiver baseline distance. Positive θ_t/θ_r is measured from x-z plane towards y-axis. Positive ϕ_t/ϕ_r is measured anti-clockwise in x-z plane.

In 2-PolSK, we consider a source symbol s with average energy $\mathrm{E}[s^H s] = 1$ is encoded in source polarization state. The

source vector is $\mathbf{s} = [s_h\ s_v]^T = \sqrt{P_t}\mathbf{E}_t s$, P_t is the transmit power, and $\mathbf{E}_t = [E_{th}, E_{tv}]^T$ is the transmit field. The received electric field is $\mathbf{E}_r = [E_{rh}, E_{rv}]^T = \sqrt{l_p}\mathbf{H}\mathbf{s}$, where l_p is the path loss, and $\mathbf{H} = [h_{hh}\ h_{hv}; h_{vh},\ h_{vv}]$ is the polarization sensitive scattering channel. The receiver contains two detectors with horizontally and vertically polarized analyzers [13]. The received electrical signal after detection is

$$\mathbf{x} = \sqrt{R}\mathbf{E}_r + \mathbf{n} \tag{1}$$

where $\mathbf{x} = [x_h, x_v]^T$ is the received symbol vector, R denotes the effective optical to electrical conversion ratio and $\mathbf{n} = [n_h, n_v]^T$ is additive white Gaussian noise vector with $n_h, n_v \sim \mathscr{C}\mathscr{N}(0, \sigma_n^2)$. The resultant electrical signal is used to obtain the polarization orientation angle of the beam as

$$\psi_r = 0.5 \tan^{-1}(I_{r2}/I_{r1}) \tag{2}$$

where $I_{r1} = x_h x_h^* - x_v x_v^*$ and $I_{r2} = x_h x_v^* + x_h^* x_v$ are the Stokes parameters. Finally, the obtained polarization parameters are de-mapped to the corresponding symbols.

III. Scattering Channel Characterization

Light propagation in scattering channel is described in terms of amplitude scattering matrix $\mathbf{S}$ which depends on the scatterer radius r_s, scatterer refractive index m, wavelength λ, scattering angle θ, and azimuth angle ϕ with respect to scattering plane [8], [14]. Thus for scattering order N, $\mathbf{H} = \prod_{n=1}^{N} \mathbf{S}$. In NLOS scattering channel, scattering direction, distance, and order are random quantities. Therefore, channel is statistically characterized in terms of XPD which accounts for energy transfer between the orthogonal polarization states. Using $\mathbf{H}$, instantaneous horizontal and vertical XPD are defined as

$$\text{XPD}_h = |h_{hh}|^2/|h_{vh}|^2, \quad \text{XPD}_v = |h_{vv}|^2/|h_{hv}|^2. \tag{3}$$

From the definition we observe that, the higher the XPD value, lesser the variance the corresponding polarization observes in the scattering environment. Considering Remark 1, we define $E_{th} = \cos\psi_t$ and $E_{tv} = \sin\psi_t$, where ψ_t is the transmit polarization orientation angle. Also, we express channel matrix parameters in polar form as $h_{hh} = |h_{hh}|e^{j\phi_{hh}}$, $h_{hv} = |h_{hv}|e^{j\phi_{hv}}$, $h_{vh} = |h_{vh}|e^{j\phi_{vh}}$ and $h_{vv} = |h_{vv}|e^{j\phi_{vv}}$. Expressing the received Stokes parameters in terms of transmit field and channel parameters as

$$\begin{aligned} I_{r1} = &\left[\{|h_{hh}|^2 - |h_{vh}|^2\}\cos^2\psi_t + \{|h_{hv}|^2 - |h_{vv}|^2\}\sin^2\psi_t \right. \\ &+ 2\cos\psi_t \sin\psi_t \{|h_{hh}||h_{hv}|\cos(\phi_{hh} - \phi_{hv}) \\ &\left. - |h_{vh}||h_{vv}|\cos(\phi_{vh} - \phi_{vv})\}\right]\cos^2\alpha_1, \end{aligned} \tag{4}$$

$$\begin{aligned} I_{r2} = &\ 2\left[|h_{hh}||h_{vh}|\cos^2\psi_t\cos(\phi_{hh} - \phi_{vh}) + |h_{hv}||h_{vv}|\right. \\ &\times \sin^2\psi_t\cos(\phi_{hv} - \phi_{vv}) + \cos\psi_t\sin\psi_t\,(|h_{hh}||h_{vv}| \\ &\left. \times \cos(\phi_{hh} - \phi_{vv}) + |h_{12}||h_{21}|\cos(\phi_{hv} - \phi_{vh}))\right]\cos^2\alpha_1. \end{aligned} \tag{5}$$

α_1 is the projection angle defined in Section V-C. Using (2), (4), and (5), and substituting $\psi_t = 0$ and $\frac{\pi}{2}$, we obtain received polarization orientations ψ_{rh} and ψ_{rv} for transmitted horizontal and vertical polarized signals respectively as

$$\begin{aligned} \psi_{rh} &= 0.5\tan^{-1}\left[\{2\sqrt{\text{XPD}_h}\cos(\phi_{hh} - \phi_{vh})\}/\{\text{XPD}_h - 1\}\right], \\ \psi_{rv} &= 0.5\tan^{-1}\left[\{2\sqrt{\text{XPD}_v}\cos(\phi_{hv} - \phi_{vv})\}/\{1 - \text{XPD}_v\}\right]. \end{aligned} \tag{6}$$

ψ_{rh} and ψ_{rv} depend on the NLOS path directions in the channel. Therefore, based on the propagation channel statistics, the variance of ψ_{rh} and ψ_{rv} may differ. Considering this aspect, in the next section we propose a detection strategy to enhance performance of UV NLOS communication system.

IV. Optimal 2-PolSK Decoding Thresholding

This section outlines the requirement of optimal thresholding and computation of optimum threshold pair.

A. Different Scenarios in Scattering Communication

Conventional polarization detection technique performs scalar product of the received Stokes vector with all the signal vectors that constitute the constellation to find the maximum [15]. So, for 2-PolSK, the Poincare sphere is divided into two symmetrical halves, i.e., symmetric thresholding is used for detection [16]. However, due to the asymmetric nature of the scattering channel, the horizontal and vertical components experience different XPDs, and symmetric thresholding may not be optimal. Thus, we propose optimal thresholding based on the statistical channel parameters σ_h^2 and σ_v^2, which denote the respective variances of the received polarization when horizontal and vertical polarization are transmitted. Based on the choice of thresholding, the following cases are observed in the scattering channel in terms of σ_h^2 and σ_v^2:

- *A* If (a) $\sigma_h^2 = \sigma_v^2$, or (b) $\sigma_h^2 > \sigma_v^2$ or $\sigma_h^2 < \sigma_v^2$, but the extreme values in the distribution are in $\sigma_h^2 \in [-\frac{\pi}{4}, \frac{\pi}{4}]$ and $\sigma_v^2 \in [\frac{\pi}{4}, \frac{3\pi}{4}]$, symmetric thresholds are sufficient, i.e., $T_1 = \frac{\pi}{4}$ and $T_2 = \frac{3\pi}{4}$.
- *B* If $\sigma_h^2 < \sigma_v^2$, and the extreme values in the distribution of σ_v^2 crosses the region $[\frac{\pi}{4}, \frac{3\pi}{4}]$, then the optimum thresholds $T_1, T_2 \in [\frac{\pi}{4}, \frac{3\pi}{4}]$ through 0.
- *C* If $\sigma_h^2 > \sigma_v^2$, and the extreme values in the distribution of σ_h^2 crosses the region $[\frac{\pi}{4}, \frac{3\pi}{4}]$, then the optimum thresholds $T_1, T_2 \in [\frac{\pi}{4}, \frac{3\pi}{4}]$ through $\frac{\pi}{2}$.

Case A is encountered when the scattering channel density is less and scattering angles, transmitter/receiver elevation and azimuth angles are small (hazy channel conditions). *Cases B* and *C* pertain to scenarios with large scattering angles and scattering density (smoky channel conditions), and is observed frequently and constitutes part of particulate matter (PM_1).

B. Distribution Parameter Estimation

We now model the received polarization distributions from the EFMC simulation data to characterize the scattering channel. We observed that the simulated data resemble fairly a Gaussian shape. Thus, Gaussian modeling is done with the objective of covering the significant extreme points in the distribution. The significance of polarization orientation depends on the values of the relative probability density function (PDF) corresponding to the horizontal and vertical transmit polarization. However, as ψ is defined on a circular scale, i.e., the values repeat after an integral multiple of π, the Gaussian distribution is suitably truncated in the range k_1 and k_2. The PDF of truncated Gaussian model (TGM) is

$$f_p(x|p, k_1, k_2) = \{\phi\left((x - \mu_p)/\sigma_p\right)\}/\sigma Z_p \tag{7}$$

where $\phi \sim \mathcal{N}(0,1)$, $p \in \{h, v\}$ indicates the transmitted signal polarization, $Z_p = \Phi(\beta_p) - \Phi(\alpha_p)$ is the normalization constant, $\alpha_p = \frac{k_1-\mu_p}{\sigma_p}$ and $\beta_p = \frac{k_2-\mu_p}{\sigma_p}$, μ_p and σ_p^2 are the mean and variance to be estimated, and $\Phi(x) = 0.5\left(1 + \text{erf}\left(x/\sqrt{2}\right)\right)$. The log-likelihood function for the entire dataset $\{x_1, x_2, \cdots, x_N\}$ is given as

$$\begin{aligned}\ln L(\{x_i\}; \mu_p, \sigma_p) =& \sum_{i=1}^{N}\left[\ln\phi\left(\frac{x_i-\mu_p}{\sigma_p}\right) - \ln\sigma_p - \log Z_p\right] \\ =& -\frac{N}{2}\log(2\pi) - N\log\sigma_p - \sum_{i=1}^{N}\frac{(x_i-\mu_p)^2}{2\sigma_p^2} - N\log Z_p.\end{aligned} \tag{8}$$

To estimate optimum μ_p and σ_p, we seek to maximize (8) and the corresponding optimization problem is formulated as

$$\begin{aligned}(\mathbf{P}1): \quad & \max_{\mu_p, \sigma_p} \ln L(\{x_i\}; \mu_p, \sigma_p) \\ \mathbf{C}1: \quad & \sigma_p > 0.\end{aligned} \tag{9}$$

(**P**1) is nonlinear. The solution employs the EM algorithm to obtain the optimal model parameters. The mean and variance of the EFMC simulated channel data are used to initialize the algorithm. The algorithm steps are as follows:

1) **E**-step: Given current estimates $\mu_p^{(t)}$ and $\sigma_p^{(t)}$, the expected values (adjustments) for mean and variance that account for the missing tails are:
   - Mean adjustment: $\Delta\mu_p = (\phi(\alpha_p^{(t)}) - \phi(\beta_p^{(t)}))/Z_p^{(t)}$
   - Variance adjustment: $\Delta\sigma_p = \frac{\alpha_p^{(t)}\phi(\alpha_p^{(t)}) - \beta_p^{(t)}\phi(\beta_p^{(t)})}{Z_p^{(t)}} + 1 - \Delta\mu_p^2$ where $\alpha_p^{(t)} = (k_1 - \mu_p^{(t)})/\sigma_p^{(t)}$, $\beta_p^{(t)} = (k_2 - \mu_p^{(t)})/\sigma_p^{(t)}$, and $Z_p^{(t)} = \Phi(\beta_p^{(t)}) - \Phi(\alpha_p^{(t)})$.
2) **M**-step: Using the adjustments from the E-step we update μ_p and σ_p in a way that increases the likelihood.
   - Update μ_p: $\mu_p^{(t+1)} = \mu_p^{(t)} - \sigma_p^{(t)} \cdot \Delta\mu_p$
   - Update σ_p: $\sigma_p^{(t+1)} = \{\sum_{i=1}^{N}(x_i - \mu_p^{(t+1)})^2/N\Delta\sigma_p\}^{\frac{1}{2}}$
3) Convergence: The algorithm iterates between the E and M steps until the changes in μ_p and σ_p are less than a tolerance level, or a maximum iteration count is reached.

These optimum modeled parameters are used to determine the optimal signal thresholds, as discussed below.

Remark 2. *Probabilistic modeling of the received polarization orientation distribution can be done using the truncated Gaussian mixture model (TGMM) as well. The choice between TGMM and TGM is purely based on the trade-off between modeling accuracy and computational complexity. We observed that TGM achieves modeling accuracy close to that of the TGMM with significantly lower computational complexity.*

C. Estimation of Optimal 2-PolSK Decoding Thresholding

For mathematical tractability, we divide the domain set of decision boundary in two subsets of range $[0, \frac{\pi}{2}]$ and $[\frac{\pi}{2}, \pi]$ and minimize the error probability for both regions separately to find the optimum thresholds individually. The probability of error for the subset in the range $[0, \frac{\pi}{2}]$ is given by

$$P_{e1} = p(v)\int_0^{T_1} f_v(y|v)dy + p(h)\int_{T_1}^{\pi/2} f_h(y|h)dy \tag{10}$$

where $p(v)$ and $p(h)$ are the steady-state probabilities of vertical and horizontal polarization, respectively. Solving

$$\frac{\partial P_{e1}}{\partial T_1} = \frac{p(v)e^{-\frac{1}{2}\left(\frac{T_1-\mu_v}{\sqrt{2}\sigma_v}\right)^2}}{\sqrt{2\pi}K_v\sigma_v} - \frac{p(h)e^{-\frac{1}{2}\left(\frac{T_1-\mu_h}{\sqrt{2}\sigma_h}\right)^2}}{\sqrt{2\pi}K_h\sigma_h}, \tag{11}$$

$$K_p = \left[\text{erf}\left(\pi/2 - \mu_p/\sqrt{2}\sigma_p\right) - \text{erf}\left(-\mu_p/\sqrt{2}\sigma_p\right)\right]. \tag{12}$$

Putting $\partial P_{e1}/\partial T_1 = 0$ and solving we get,

$$((T_1 - \mu_v)/\sigma_v)^2 - ((T_1 - \mu_h)/\sigma_h)^2 = M_1, \tag{13}$$

where $M_1 = 2\ln\left[\frac{\sigma_v p(v) K_1}{\sigma_h p(h) K_2}\right]$. Solving for T_1 we get,

$$\begin{aligned}T_1^{opt} =& \{\pm 2\left[(\mu_h\sigma_v^2 - \mu_v\sigma_h^2)^2 - (\mu_v^2\sigma_h^2 - \mu_h^2\sigma_v^2 - M_1)\right. \\ & \left.\times(\sigma_h^2 - \sigma_v^2)\right]^{1/2} - 2(\mu_h\sigma_v^2 - \mu_v\sigma_h^2)\}/(2(\sigma_h^2 - \sigma_v^2)).\end{aligned} \tag{14}$$

Among the two values of T_1^{opt}, the value $\in [0, \pi]$ is selected. Probability of error for the subset in the range $[\pi/2, \pi]$ is obtained similarly by minimizing

$$P_{e2} = p(v)\int_{\pi/2}^{T_2} f_v(y|v)dy + p(h)\int_{T_2}^{\pi} f_h(y|h)dy. \tag{15}$$

The expression for T_2^{opt} is the same as that given in (14) with μ_h replaced by $\mu_h + \pi$ and M_1 replaced by

$$M_2 = 2\ln\left[\frac{\sigma_v p(v)\left[\text{erf}\left(\frac{\pi-\mu_v}{\sigma_v}\right) - \text{erf}\left(\frac{\pi/2-\mu_v}{\sigma_v}\right)\right]}{\sigma_h p(h)\left[\text{erf}\left(\frac{\pi-\mu_h}{\sigma_h}\right) - \text{erf}\left(\frac{\pi/2-\mu_h}{\sigma_h}\right)\right]}\right]. \tag{16}$$

T_1^{opt} and T_2^{opt} are used for the received polarization detection.

V. Electric Field Monte Carlo (EFMC) Simulation

In this section, we discuss EFMC simulation method for the propagation of polarized light in the optical scattering channel to verify the performance of optimal thresholding scheme.

A. Photon Propagation and Field Updation

EFMC is based on tracing the scattered electric field to simulate polarized light propagation. Scattering takes place in local coordinate system (**p**, **q**, **r**) at each iteration step. **p** and **q** are the unit vectors along electric field parallel and perpendicular components and **r** is the photon scattering direction prior to current scattering. The scattering (θ) and azimuth (ϕ) angles are measured with respect to the direction of incidence of photon on the scatterer. Therefore, the update rule at each scattering is governed by $[\mathbf{p}'\ \ \mathbf{q}'\ \ \mathbf{r}'] = A(\theta, \phi)[\mathbf{p}\ \ \mathbf{q}\ \ \mathbf{r}]$ where

$$A(\theta, \phi) = \begin{bmatrix}\cos\phi & \sin\phi\sin\theta & \sin\phi\cos\theta \\ 0 & \cos\theta & -\sin\theta \\ -\sin\phi & \sin\theta\cos\phi & \cos\theta\cos\phi\end{bmatrix}. \tag{17}$$

The position of i-th scatterer is updated as $\mathbf{s}_i = \mathbf{s}_{i-1} + d_{i-1}\mathbf{r}_{i-1}$, with $\mathbf{s}_1 = \mathbf{s}_T + d_0\mathbf{r}_0$. For the i-th scattering, the scattering plane is spanned by $\mathbf{r}_{i-1}$ and $\mathbf{r}_i$. For $i \geq 1$, the scattering angle is

$$f_\theta(\theta_i) = \{{k_s}^R f_\theta{}^R(\theta_i) + {k_s}^M f_\theta{}^M(\theta_i)\}/k_s, \quad 0 \leq \theta_i \leq \pi. \tag{18}$$

$k_s = {k_s}^R + {k_s}^M$, ${k_s}^R$ and ${k_s}^M = N_d Q_s \pi r_s^2$ are the molecule (Rayleigh) and aerosol (Mie) scattering coefficient, respectively. Q_s is the scattering cross section [17]. Rayleigh

TABLE I SIMULATION PARAMETERS

Variable	Value	Variable	Value	Variable	Value
β_t	10^o	A_r	1.77 cm^2	P_t	20 mW
m	1.5	λ	250 nm	N	1
r_s	280 nm	N_d	10^9 m^{-3}	f [18]	0.72
ϕ_t, ϕ_r	0°	k_s^R	0.328 km^{-1}	γ [18]	0.0172
d	800 m				

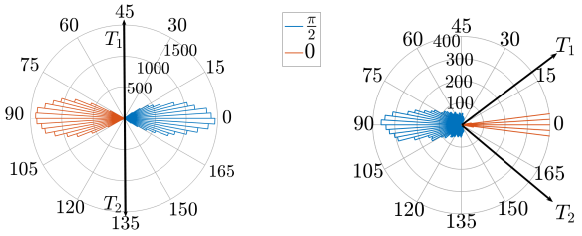

(a) $\theta_t = 40^\circ, \theta_r = 140^\circ$ (b) $\theta_t = 45^\circ, \theta_r = 135^\circ$

Fig. 2 Two different example scattering channel scenarios considered with simulation parameters in Table I: (a) Case A, (b) Case B.

and Mie phase functions ($f_\theta{}^R(\theta_i)$, $f_\theta{}^M(\theta_i)$) are given in [18] where γ and f are model parameters. Propagation distance is distributed as $f_d(d_i) = k_e e^{-k_e d_i}, 0 \leq d_i \leq \infty$, $k_e = k_s + k_a$ is the extinction coefficient and k_a is attenuation coefficient.

B. Photon Reception and Polarization Detection

The detector response is independent of polarization. The photon is detected if the following conditions are satisfied: (i) $\cos^{-1}(\mathbf{a}_r.(-\mathbf{r}_i)) \leq \beta_R/2$, ($ii$) $d_i < l_m$, (iii) $||\mathbf{s}_i + d_i\mathbf{r}_i||_2 \leq A_r$. $\mathbf{a}_r = A(\theta_r, \phi_r)[0\ \ 0\ \ 1]^T$ is the receiver direction cosine, l_m is the mean free path of photon and A_r is the optical receiver area. (i) ensures that i-th scatterer lies in receiver FOV and depends on the receiver material property, (ii) ensures that the photon does not meet any scatterer in FOV before reaching the receiver, and (iii) ensures that the photon falls within A_r.

As polarization is a vector property of the electromagnetic wave, the polarization plane of the i-th received photon is projected on the receiver plane such that $\mathbf{E}_r = \begin{bmatrix} E_{hi} & E_{vi} \end{bmatrix}^T \cos\alpha_1$, where $\alpha_1 = \frac{\mathbf{a}_r \cdot \mathbf{r}_i}{|\mathbf{a}_r||\mathbf{r}_i|}$ is the angle between the polarization plane of the received photon and the receiver plane. From $\mathbf{E}_r$, Stokes parameters are obtained which gives the detected photon polarization. As reported in [19], the turbulence effects on polarization are considered negligible compared to the scattering in optical channel over short ranges.

VI. Results and Discussion

In this section, we analyze the XPD-aware scattering channel characteristics and study the benefit of optimal thresholding for improved BER performance. Our conducted EFMC simulations are based on the parameters listed in Table I.

A. Performance in Two Different Channel Scenarios

Figs. 2(a) and 2(b) show the EFMC simulation data of ψ_r when horizontal and vertical polarized signals are transmitted for respectively $\theta_t = \pi - \theta_r = 40^\circ$ and 45°. For the parameters in Table I, these two cases are observed. Fig. 2(a) corresponds to *Case A* as two distributions are far apart and

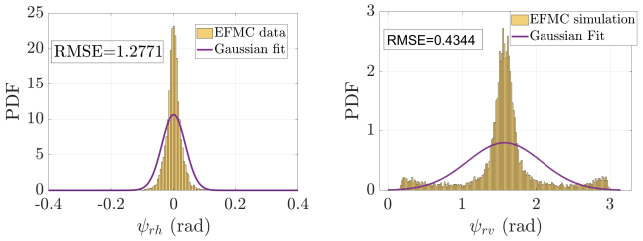

(a) $\psi_t = 0$ (b) $\psi_t = \frac{\pi}{2}$

Fig. 3 Distribution of received polarization orientation angle ψ_r.

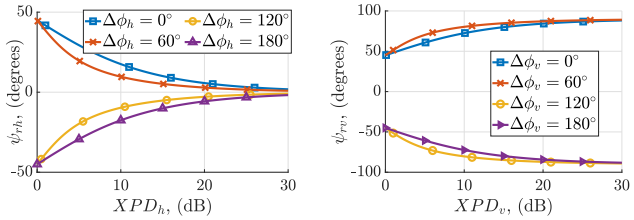

(a) $\psi_t = 0$ (b) $\psi_t = \frac{\pi}{2}$

Fig. 4 Variation of received polarization orientation ψ_r with XPD.

symmetric thresholds are optimum. However, in Fig. 2(b), corresponding to *Case B*, variance corresponding to vertical polarization is large such that it crosses the region $[\pi/4, 3\pi/4]$, whereas variance of horizontal polarization lies within $[\pi/4, 3\pi/4]$. Henceforth, we consider the *Case B* for performance optimization via optimal thresholding scheme proposed above.

B. Comparison of Original and Modeled Distribution

Figs. 3(a) and 3(b) show the distribution of ψ_r and TGM for them when horizontal and vertical polarization were transmitted, respectively for *Case B* considered in Fig. 2(b). Distributions are generated for FOV $= 30^o$ and SNR $= 36$ dB. Note that Gaussian modeling is still done as the distribution in (7) takes the mean and variance of the Gaussian distribution which is truncated. Additionally, the values in the Poincare sphere which lie in the other half are truncated. For example, the values of $\psi_r \notin [\pi/4, 3\pi/4]$ are excluded before modeling.

Remark 3. *To keep the distribution of ψ_r symmetric about 0 and $\frac{\pi}{2}$ radians, we plot distribution for ψ_{rh} and ψ_{rv} in the range $[\frac{-\pi}{2}, \frac{\pi}{2}]$ and $[0, \pi]$ respectively, as shown in Fig. 3.*

C. Variation of Polarization Orientation with XPD

The variation of ψ_r with channel XPD defined in (6) are shown in Figs. 4(a) and 4(b) for different values of $\Delta\phi_h = \phi_{hh} - \phi_{vh}$ and $\Delta\phi_v = \phi_{hv} - \phi_{vv}$ when transmit polarization is respectively horizontal and vertical. When horizontal polarization is transmitted, for XPD$_h = 0$ dB, equal power is divided between the horizontal and vertical component, i.e., $\psi_{rh} = \frac{\pi}{4}$. As XPD improves, ψ_{rh} decreases, reducing to zero at large XPD values. Similar trend is observed for vertical polarization orientation with increase in vertical channel XPD.

D. Impact of Change in Elevation Angle

As polarization is direction-sensitive, the impact of elevation angle on channel XPD and variance of ψ_r are also observed,

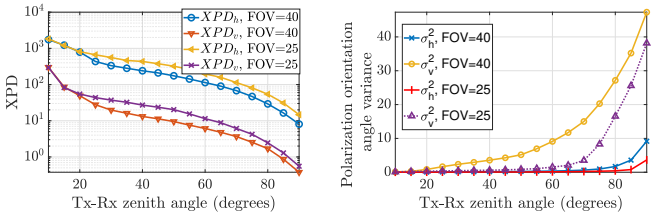

(a) (b)

Fig. 5 Impact of change in elevation angle on (a) XPD, (b) σ^2_{rh}, σ^2_{rv}.

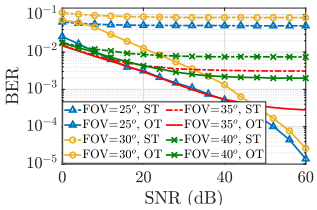

Fig. 6 BER versus SNR performance for different receiver FOV. ST: Symmetric thresholding, OT: Optimal thresholding.

as shown in Figs. 5(a) and 5(b). For $\theta_t = \pi - \theta_r$, as the elevation angle increases, average XPD_h and XPD_v decreases, and σ^2_{rh} and σ^2_{rv} increases. Also, for larger FOV, lower value of XPD and a higher variance in ψ_r are observed, which is due to an increase in number of photons received with more deviated polarization compared to the reference polarization. Additionally, $\text{XPD}_v < \text{XPD}_h$ is observed; the difference is entirely dependent on the channel parameters considered. For these XPD values, $\sigma^2_{rv} > \sigma^2_{rh}$; the chances of polarization being randomly received increases at higher elevation angles as the source and receiver move away from the LOS condition. Also, the variance of ψ_r decreases with increase in XPD, indicating an improved polarization scattering channel.

E. BER Performance

Fig. 6 captures the comparative performance of the proposed optimal thresholding with conventional symmetric thresholding in terms of BER for different FOV with $\theta_t = \pi - \theta_r = 45°$. The BER curves are observed to show different trends with optimal thresholding for detection. At high signal-to-noise ratio (SNR) values, BER $\to 0$ for small FOV and saturates for large FOV. In the first case, BER depends on the receiver noise; thus optimal thresholding correctly detects horizontal and vertical polarization in absence of receiver noise. However, in the second case, BER is additionally affected by the scattering channel. Channel condition is such that both horizontal and vertical polarization states have the possibility of achieving same polarization orientation, i.e., there exists no such threshold pair which could make BER zero even in the absence of noise. Therefore, due to channel scattering, BER tends to saturate at a large SNR values. This situation is observed in several scenarios, such as at large elevation angles, scattering orders, size parameter, beam divergence angle, or receiver FOV. Intuitively, at large FOV, the BER decreases, though optimal thresholding still performs much better.

VII. Conclusion

The study in this paper has revealed that signal polarization-dependent channel XPD plays a crucial role in optimal thresholding for efficient polarization multiplexed signal communication over the UV scattering channels. Through mathematical characterization of XPD and analysis of received polarization distributions for orthogonally polarized input signals XPD-dependent thresholding parameter has been optimized in 2-PolSK transmission. Through EFMC simulation of various UV scattering channels significant performance gain of optimal thresholding-based symbol detection with respect to the conventional symmetric thresholding-based approach has been demonstrated. The findings of this study will be useful in increasing the capacity of the UV scattering channels for polarization multiplexed transmissions.

References

[1] Z. Jiang, *et al.*, "Achievable rates and signal detection for photon-level photomultiplier receiver based on statistical non-linear model," *IEEE Trans. Wirel. Commun.*, vol. 18, no. 12, pp. 6015–6029, 2019.

[2] T. Cao, T. Wu, C. Pan, and J. Song, "Performance of multipulse pulse-position modulation in nlos ultraviolet communications," *IEEE Commun. Lett.*, vol. 27, no. 3, pp. 901–905, 2023.

[3] C. Xu and H. Zhang, "Packet error rate analysis of IM/DD systems for ultraviolet scattering communications," in *Proc. IEEE MILCOM*, 2015.

[4] Y. Zhao, *et al.*, "Investigation of characteristics of ultraviolet light pulse weak signal communication system based on fourth-order frequency-shift keying modulation," in *Photonics*, vol. 11, no. 5, 2024, p. 395.

[5] S. Arya and Y. H. Chung, "High-performance and high-capacity ultraviolet communication with orbital angular momentum," *IEEE Access*, vol. 7, pp. 116 734–116 740, 2019.

[6] L.Wang, *et al.*, "Non-line-of-sight ultraviolet link loss in noncoplanar geometry," *Optics letters*, vol. 35, no. 8, pp. 1263–1265, 2010.

[7] M. Noshad, M. Brandt-Pearce, and S. G. Wilson, "NLOS UV communications using M-ary spectral-amplitude-coding," *IEEE Trans. Commun.*, vol. 61, no. 4, pp. 1544–1553, 2013.

[8] M. Xu, "Electric field monte carlo simulation of polarized light propagation in turbid media," *Opt. Express*, vol. 12, no. 26, pp. 6530–6539, Dec 2004.

[9] A. Doronin, A. J. Radosevich, V. Backman, and I. Meglinski, "Two electric field monte carlo models of coherent backscattering of polarized light," *J. Opt. Soc. Am. A*, vol. 31, no. 11, pp. 2394–2400, Nov 2014.

[10] L. Li , *et al.*, "Simulation of light scattering from a colloidal droplet using a polarized monte carlo method: application to the time-shift technique," *Opt. Express*, vol. 27, no. 25, pp. 36 388–36 404, Dec 2019.

[11] H. Yin, *et al.*, "Vectorized polarization-sensitive model of non-line-of-sight multiple-scatter propagation," *J. Opt. Soc. Am. A*, vol. 28, no. 10, pp. 2082–2085, Oct 2011.

[12] ——, "Extending the data rate of non-line-of-sight UV communication with polarization modulation," in *Unmanned/Unattended Sensors and Sensor Networks IX*, vol. 8540. SPIE, 2012, p. 85400I.

[13] Z. Hailiang *et al.*, "Characteristics of non-line-of-sight polarization ultraviolet communication channels," *Appl. Opt.*, vol. 51, no. 35, pp. 8366–8372, Dec 2012.

[14] W. J. Wiscombe, "Improved mie scattering algorithms," *Appl. Opt.*, vol. 19, no. 9, pp. 1505–1509, May 1980.

[15] S. Benedetto and P. Poggiolini, "Multilevel polarization shift keying: optimum receiver structure and performance evaluation," *IEEE Trans. Commun.*, vol. 42, no. 234, pp. 1174–1186, 1994.

[16] ——, "Theory of polarization shift keying modulation," *IEEE Transactions on Communications*, vol. 40, no. 4, pp. 708–721, 1992.

[17] C. Xu, H. Zhang, and J. Cheng, "Effects of haze particles and fog droplets on NLOS ultraviolet communication channels," *Opt. Express*, vol. 23, no. 18, pp. 23 259–23 269, Sep 2015.

[18] R. Yuan, J. Ma, P. Su, Y. Dong, and J. Cheng, "Monte-carlo integration models for multiple scattering based optical wireless communication," *IEEE Trans. Commun.*, vol. 68, no. 1, pp. 334–348, 2020.

[19] J. Zhang, *et al.*, "Theoretical and experimental studies of polarization fluctuations over atmospheric turbulent channels for wireless optical communication systems," *Opt. Express*, vol. 22, no. 26, pp. 32 482–32 488, Dec 2014.